Journal of Applied Polymer Science

Piezoelectric Coaxial Filaments Produced by Coextrusion of Poly(vinylidene fluoride) and Electrically Conductive Inner and Outer Layers

Rui S. Martins,[1] Renato Gonçalves,[2] Tiago Azevedo,[1] José G. Rocha,[3] João M. Nóbrega,[1] Helder Carvalho,[4] Senentxu Lanceros-Mendez[2]

[1]IPC/I3N—Institute for Polymers and Composites, University of Minho, Campus de Azurém, Guimarães 4800-058, Portugal
[2]Centro/Departamento de Física, University of Minho, Campus de Gualtar, Braga 4710-058, Portugal
[3]Department of Industrial Electronics, University of Minho, Guimarães 4800-058, Portugal
[4]Department of Textile Engineering, University of Minho, Campus de Azurém, Guimarães 4800-058, Portugal
Correspondence to: H. Carvalho (E-mail: helder@det.uminho.pt)

ABSTRACT: The development of new thermoplastic polymer-based piezoelectric sensors with filament geometry is described. These filaments are appropriate for integration into textiles and provide new possibilities in the design and development of low-cost flexible sensors produced at high rates. The developed three-layered piezoelectric monofilaments have been produced by coextrusion using poly(vinylidene fluoride) and two different polypropylene-based electrically conductive polymers. Filaments with about 800-μm diameter, producing electrical signals proportional to the mechanical deformation applied, were obtained. The signal output has been found adequate for straightforward use with conventional piezoelectric signal conditioning systems. One of the conductive polymers tested allowed better filament geometry and process stability. This article describes the coextrusion production process and the results obtained in the electromechanical tests performed. © 2014 Wiley Periodicals, Inc. J. Appl. Polym. Sci. **2014**, *131*, 40710.

KEYWORDS: conducting polymers; extrusion; fibers; piezoelectric; PVDF; sensors and actuators; textiles

Received 14 October 2013; accepted 2 March 2014
DOI: 10.1002/app.40710

INTRODUCTION

Poly(vinylidene fluoride) (PVDF) has been extensively studied due to its remarkable piezoelectric, pyroelectric, and ferroelectric properties among polymers. These properties have been used for the development of sensor and actuator devices and technologies.[1–3]

The electroactive properties of PVDF depend on several factors including the degree of crystallinity, structure, and orientation of the crystalline fraction of the semicrystalline polymer, which strongly depend on the used processing conditions.[1,3–12]

PVDF can crystallize in four different crystalline phases, identified as α, β, γ, and δ. The nonpolar α-phase is readily obtained by crystallization from the melt at high or moderate cooling speeds.[1,3] From the point of view of its piezoelectric activity, the most interesting phase is the β-phase, which is most commonly obtained by drawing the α-PVDF at temperatures between 80 and 120°C with a draw ratio (R) between 3 and 5.[1,11,12]

After processing, the material is usually further poled to improve its piezoelectric response, aiming for the production of better sensor and actuator devices. After this stage, the piezoelectric polymer will produce an electrical potential on mechanical excitation, and a mechanical action will be produced if the polymer is subjected to an electric field. Poling can be achieved using several alternatives, including corona poling and the Bauer method, among others.[1–3] The most simple and straightforward poling method is performed just by applying to the electroded material an electrical field higher than its coercive field, which typically ranges from 50 to 120 MV m^{-1} for PVDF.[13] If the poling is undertaken in a temperature range between 85 and 130°C, the piezoelectric response can be further improved.[14]

PVDF-based piezoelectric sensors and actuators are available on the market, usually in the form of films. A polymer-based piezoelectric device is composed of at least one piezoelectric active layer and two electrically conductive layers, used as electrodes for the connection of electronic conditioning/drive equipment.[15]

In the case of films, the typical arrangement of the layers is the parallel one (see Figure 1). In this work, piezoelectric filaments comprising three thermoplastic material layers in coaxial

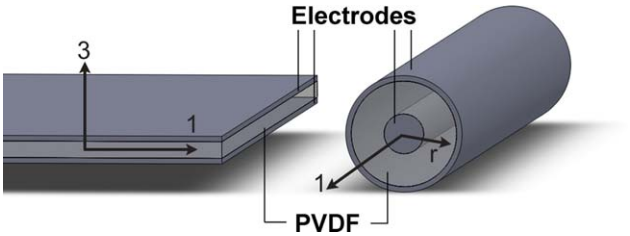

Figure 1. Parallel (film) and coaxial (filament) arrangement of layers with relevant mechanical and electrical axes. [Color figure can be viewed in the online issue, which is available at wileyonlinelibrary.com.]

arrangement, as illustrated in Figure 1, have been developed. This geometry is expected to allow a new range of applications in areas such as e-textiles and structural health monitoring.

An effective way to achieve the desired geometry is to process simultaneously the conductive elements and the piezoelectric layer. One of the most interesting possibilities is the use of polymer-based electrodes, in particular, the ones based on polypropylene. Polypropylene has a very competitive cost, based on the cheap monomer and the efficient polymerization technology, when compared with other polymers.[16] It can be easily processed by extrusion and the addition of a small amount of conductive fillers, allows the achievement of electrically conductive thermoplastic composites.[17] Several thermoplastic polymer-based conductive grades are commercially available.

The extrusion of PVDF in the form of filament and the relationship between processing parameters and the β-phase content has been investigated in some works. Some authors have concluded that the optimized processing conditions for single PVDF monofilaments are similar to the ones established for film extrusion, that is, drawing the α-PVDF at temperatures between 80 and 120°C using a draw ratio between 3 and 5.[11,12,18,19] The influence of melt draw ratio and draw ratio in a latter cold drawing step at 80°C have been previously investigated by Lund and Hagström.[20] It has been shown that the cold drawing step is necessary to obtain filaments with β-crystallinity, regardless of the melt draw ratio, which in turn influences the crystallinity of the polymer.

For the production of multilayered filaments (see Figure 1), some studies have been focused on the investigation of the influence of a conductive inner core on the β-phase content of PVDF. In one study, filaments have been coextruded with a Polypropylene/Carbon-Black conductive inner core and a PVDF outer layer, and it has been shown that the electroactive phase content is not affected by the presence of the conductive inner core and in fact, depends just on the drawing temperature and ratio, as previously stated for monomaterial filaments.[21] Similar work has been reported for PP-CB filaments and for a PP compound containing 10 wt % of carbon nanotubes.[22,23]

With respect to the electroactive properties of the extruded filaments, a piezoelectric cable obtained from a two layer coextruded filament, comprising an internal semiconductive electrode and a PVDF layer, coated with a thin layer of a semiconductive copper-based lacquer, was tested and characterized.[24] A nonlinear relationship between the electrical charge produced by the cable and the force applied was determined.

Mazurek et al. described the production of concentric piezoelectric cables by coextrusion, being the outer electrode applied in an additional step.[25] The cables were poled using four different poling methods:

- the thermoelectret method, in which PVDF is exposed to a strong electric field at a high temperature. After a defined poling time, the polymer is cooled while still exposed to the electric field;
- the breakdown method, in which the PVDF is exposed to a field stronger than 5 MV cm^{-1};
- the low-temperature plasma method, using plasma produced in a discharge through a rarified gas, with the inner conductive layer being used as second electrode;
- the Corona method, in which poling is achieved using Corona discharge.

These experiments showed that the highest values of piezoelectric coefficient were obtained using the low-temperature plasma method.

The development of piezoelectric cables using sequential processing techniques was also described.[26] An inner conductive core is covered with PVDF, which is then electroded with a metal or a semiconducting polymer, and mechanically strengthened with a polymer coating. The influence of several parameters on the β-phase content of PVDF such as processing temperature, draw ratio, and cooling temperature of the PVDF after drawing, as well as the influence of the thermal impact of the coating step used to apply the outer electrode, were studied. It was found that the β-phase content increased by from 20 to 100% when draw ratios varied between 3 and 5. A reduction of the cooling temperature from 5 to −30°C produced an increase to 100% of β-phase content, from 61 to 71%, depending on the inner core material. The thermal impact of the coating procedure resulted in a significant decrease of β-phase content, from 100% to a value varying between 79 and 49%.

Vatansever et al. report the production of PVDF monofilaments, which are stretched (draw) and poled inline by an electric field produced between two parallel plates.[27,28] A functional prototype of a sensor based on the material produced was achieved by placing a number of filaments in a parallel arrangement and providing copper electrodes on the upper and lower faces of the assembly. The assembly was shown to produce electrical signal on mechanical shock.

Walter et al. manufactured a composite product comprising PVDF filaments and epoxy resin, with the filaments laid out in a parallel arrangement. The composite was then poled with a linear electric field in a direction perpendicular to the fibers.[29] Piezoelectric activity was shown both for longitudinal and bending deformations.

Piezoelectric bicomponent fibers using PVDF and a PP/CB inner core have also been reported.[30] Poling was achieved by applying a high voltage directly to the filaments and placing the materials in an oven at 100°C. A voltage of 1 kV was used,

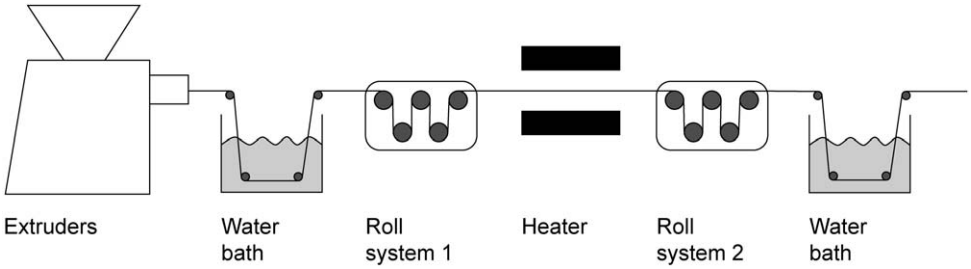

Figure 2. Monofilament prototype coextrusion line used for the production of the filaments.

which resulted in a poling field of about 56 MV m^{-1}. In a follow-up work, poling was produced using corona discharge and it was found that permanent polarization is achieved after 2 s, which represents an important advantage for industrial production.[31]

A different approach to the production of piezoelectric multilayer fibers has been taken by Egusa et al., who presented a production process involving the creation of a macroscopic preform of the fiber.[32,33] This preform is achieved by assembling the layers composing the fiber in a flat arrangement and rolling them together to produce the round preform. The preform is then drawn, reaching its final dimensions (and in the case of piezoelectric fibers, also its desired functional properties) after the drawing process. This methodology allows the production of tens of meters of fiber in each cycle, but it does not allow a continuous production of the filament. Fibers of different, very complex structures and cross sections have been used, showing a piezoelectric response and acoustic transduction from kilohertz to megahertz frequencies.

Unlike to all the works previously presented, in which the filaments are obtained in discrete production steps, in this work, the conductive and piezoelectric layers (Figure 1) are produced by coextrusion, in a single operation. This strategy represents a significant reduction of the processes involved in the manufacturing process.

The remainder of this article is organized as follows: Section Experimental describes the materials used and the production and characterization methods, whereas in Section Results and Discussion, the main results are presented and discussed. This article ends with the main conclusions of the work.

EXPERIMENTAL

Filament Production

The piezoelectric filament is composed by a PVDF layer surrounded by two conductive layers in a coaxial arrangement (Figure 1).

Two different coextruded filaments were produced using Solvay Solef Ta-1010 PVDF for the piezoelectric layer. For the electrode layers, two different compounds were used: Pre-Elec 1396 conductive PP, from Premix, and PlastiCyl PP2001, from Nanocyl.

The Pre-Elec 1396 polymer is a carbon-black filled polypropylene compound which is extruded directly as provided by the manufacturer. The datasheet specifies a volume resistivity lower than 10 Ω cm. No details on the exact composition are given. The PlastiCyl PP2001 is a carbon nanotube-based compound supplied in a 20 wt % master batch. The datasheet specifies a volume resistivity of 10 Ω cm for a compound with 5 wt %. For this work, it was diluted on a Leistritz twin-screw extrusion line, using plain PP Moplen HP540J from LyondellBasell, to achieve a 7 wt % concentration for the filler, and granulated using a conventional granulator (C F SCHEER & CIE, Model D-7000).

Although the percolation limit is specified in the material datasheet as being around 3–4 wt %, it was found that a 7 wt % concentration is required for adequate conductivity of the electrode layers, as will be shown in Section Measurement of Electrical Conductivity. This is mainly a consequence of the cold drawing step that takes place after extrusion. Actually, values of concentration at this level are not uncommon in filament spinning. For instance, a content of 10 wt % have been used with the same material in the production of thinner filaments, without affecting process stability.[23]

The two filaments will hereinafter be designated as Type 1 (extruded using the Premix compound) and Type 2 (extruded using the Nanocyl compound).

The three-layer filaments were then produced in a prototype monofilament coextrusion line schematically illustrated in Figure 2.

In this line, two extruders were used, because two different materials are required to produce the desired filaments. In the system, the materials are pumped at a predefined rate by the extruders, using the processing conditions shown in Table I, through a coextrusion die, illustrated in Figure 3, which shapes the multilayer coextruded filaments.

The modular approach of the die design allows the coextrusion of filaments comprising up to four layers. The seven modules, shown in Figure 3(a), can be replaced and their positions can be switched or rotated, to produce the desired type of filament, with a specified arrangement for the layers.

The electrically conductive material [black streamline shown in Figure 3(b)] enters the die flow channel pumped from the axially aligned extruder. This material is then divided in two independent streamlines, to form the filament's two conductive layers (the inner and outer layers). The piezoelectric material [white streamline shown in Figure 3(b)] is pumped from a perpendicularly aligned extruder. The three independent flows are then conducted to the periphery of the die, and start flowing through channels aligned in the axial direction. At the desired

Table I. Processing Conditions Used on the Production of the Filaments

Conditions	Filament Type 1	Filament Type 2
Extrusion temperature (at die) PVDF	235°C	235°C
Extrusion temperature (at die) Conductive PP	255°C	255°C
Extruder screw speed PVDF	5 rpm	5 rpm
Extruder screw speed Conductive PP	10 rpm	10 rpm
Stretch ratio	4	5
Roll system 1 speed	7.5 m min^{-1}	7.5 m min^{-1}
Roll system 2 speed	30 m min^{-1}	37.5 m min^{-1}
Water bath temperature	20°C	20°C
Heater temperature	210°C	210°C

location, all the flow fronts are sequentially conducted to the main channel, to form the filament with the desired layer arrangement.

The depressions existing in the modules that conduct the material to form an additional layer (M3 and M5) were created to assure an even distribution of the flow along the perimeter of the layer. The modules' arrangement presented in Figure 3 allows the production of the three-layer filament.

The die also features screws for layer thickness adjustments. These are screwed in Module M7, and can be used to adjust independently the flow rate of each streamline, by restricting the flow channel of the material that will form the respective layer.

After leaving the coextrusion die the filament is cooled in a water bath to room temperature. Subsequently, the material is drawn in a heater at a defined temperature, being the draw ratio (R) determined by the relation between the linear velocities v_1 and v_2, the velocity set for roll systems 1 and 2, respectively:

$$R = \frac{v_2}{v_1} \quad (1)$$

The cooling/heating steps are required to assure a more accurate control of the drawing temperature.

An extensive experimental trial allowed establishing the optimal processing conditions for the filaments, regarding process stability and final quality of the filament. The objective was to achieve the highest draw ratio possible at the ideal drawing temperature interval. Table I summarizes all the relevant processing conditions used.

The drawing temperatures used are higher than the effective suggested temperatures found in the literature (80–120°C) but it has only been possible to draw these three-layered filaments during production using relatively high temperatures for the heater (Figure 2).[1–11] Using the equipment available, the process became unstable when lower temperatures were used, with frequent filament breakage and defects. However, it should be noted that unlike in a static drawing process, in the present case the drawing is obtained inline, thus in dynamic conditions. The filament travels through the heater at a relatively high speed, and consequently has a residence time in the heater lower than 2 s. Considering the low thermal diffusivity typical for the polymeric materials, it is obvious that the PVDF layer does not reach the temperature imposed at the heater. To assess the actual content of electroactive phase of the PVDF layer, the β-phase content was determined, as described in the next section.

Determination of β-Phase Content of the Samples

β-phase of PVDF on the extruded filaments was characterized by Fourier transformed infrared spectroscopy (FTIR) using a Jasco FT-IR 4100 in attenuated total reflectance mode (ATR) over a range of 4000–600 cm^{-1} and 64 scans for each sample were accumulated. For each type of filaments, five samples were analyzed. For this characterization, 30-mm long coextruded samples were used, from which the outer layer was removed to expose the PVDF layer, which was placed directly in the ATR device. Removal of the outer layer was achieved by peeling it off with a sharp knife, which was a straightforward operation due to the weak adhesion between the different layers.

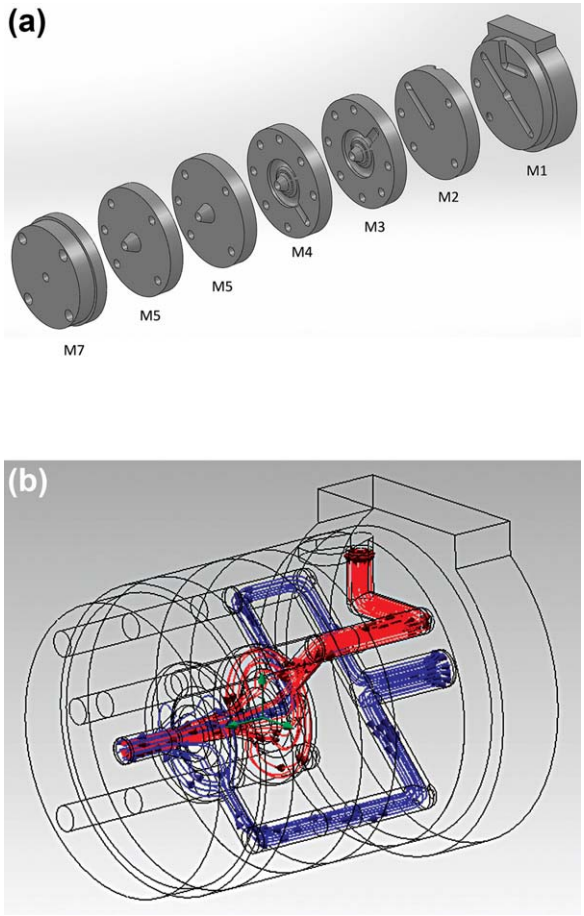

Figure 3. Schematic representation of the coextrusion functional parts: (a) exploded view and (b) coextruded materials streamlines (in black the inner and outer layers and in white the middle layer). [Color figure can be viewed in the online issue, which is available at wileyonlinelibrary.com.]

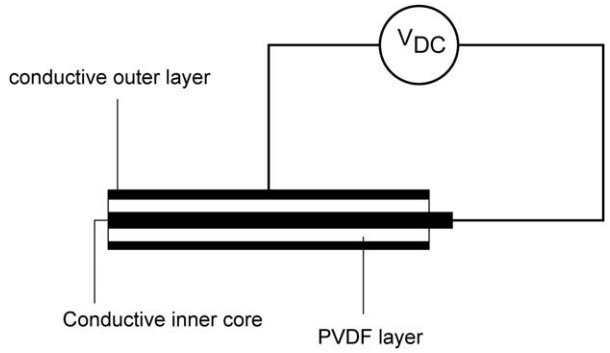

Figure 4. Poling scheme for the coextruded filament.

To quantify the amount of β-phase, infrared absorption bands at 763 and 840 cm^{-1}, specific of the α-phase and β-phase, were used.[1,34] A procedure was used, in which the β-phase content is calculated by:

$$F(\beta)=\frac{X_\beta}{X_\alpha+X_\beta}=\frac{A_\beta}{(K_\beta/K_\alpha)A_\alpha+A_\beta}=\frac{A_\beta}{1.26A_\alpha+A_\beta} \quad (2)$$

where A_α and A_β are the absorbances at 763 and 840 cm^{-1}, corresponding to the α-phase and β-phase material; K_α and K_β are the absorption coefficients at the respective wave numbers and X_α and X_β are the crystalline fraction of each phase. The value of K is 7.7×10^4 and 6.1×10^4 cm^2 mol^{-1} for the α-phase and β-phase, respectively.[1]

Filament Poling

Poling was achieved by the application of a high voltage to the filament using a direct connection. For this purpose, filaments were cut into 10-cm long segments and a high voltage source was connected between the outer and the inner conductive layer, according to the scheme presented in Figure 4. The connection was achieved by clamping crocodiles directly to the outer and inner layers of the filament.

The maximum voltage that could be applied on the filament poling experiments was about 9 kV. Above this value, short circuit of the filament due to localized breakdown of the PVDF layer occurred. To increase the effectiveness of poling, the filaments were kept inside an oven for 20 min at 80°C and then cooled to room temperature while subjected to the electrical field. Only then was the voltage source disconnected.

Mechanical Characterization

Three filament samples of each of the two filament types were stretched (drawed) until rupture in a universal testing machine (Shimadzu AG-IS 500 N) at a speed of 10 mm min^{-1}. The initial distance between grips was 30 mm.

Electrical Evaluation

Signal Conditioning and Acquisition. For the evaluation of the potential of the extruded material for sensor applications, the filaments were connected to a custom-built charge amplifier (Figure 5).

In piezoelectric sensors, an electrical potential is generated on application of mechanical action. However, the charge unbalance involved in this process is very small and is quickly dissipated in a conventional amplifier. Thus, any mechanical action produces a signal peak when the action occurs, but on achieving a static condition no additional electrical signal is produced.

To provide a piezoelectric measurement system with the ability to measure quasi-static phenomena, or to allow it to measure slow varying stimuli, a charge-to-voltage converter, commonly known as charge amplifier, is used. In this amplifier, the charge pumped into the amplifier by the piezoelectric sensor is picked up and held in the capacitor present in the amplifier's feedback loop.

Due to the presence of bias currents, a charge amplifier with only a capacitor in its feedback loop has the tendency to saturate. To avoid this, a feedback resistor is used, which conversely causes the capacitor to discharge through the feedback resistor. The discharge time to 36.8% of charge, known as the time constant, can be varied by adjusting the value of the component and is given by:

$$T=R_f C_f \quad (3)$$

where

T = capacitor discharge time constant (s)

R_f = feedback resistor value (Ω)

C_f = feedback capacitor value (F)

The time constant is just a different expression of another important parameter, which is the lower cut-off frequency of the sensor/amplifier system. In fact, the lower cut-off frequency f_{lc} can be written as:

$$f_{lc}=\frac{1}{2\pi R_f C_f} \quad (4)$$

It can be shown that using the charge amplifier, the lower cut-off frequency is just dependent of the feedback resistor and capacitor, being the influence of the sensor's own capacitance and of other parasitic capacitances, such as cable capacitances, negligible due to the high open-loop gain of the operational amplifier. A piezoelectric sensor coupled to a charge amplifier can thus be dimensioned to perform measurements of very low-frequency (or quasistatic) signals, although it is not able to measure purely static signals.[35,36]

The upper frequency limitation of a piezoelectric sensor coupled to the charge amplifier is theoretically determined only by the sensor's electromechanical properties and by the frequency response of the amplifier. However, this is only true if the resistance of the connection between the sensor and the amplifier is negligible. This is not the case in the filament sensors produced,

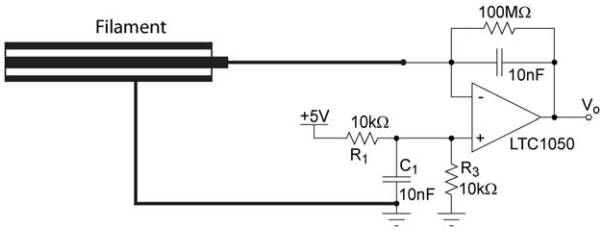

Figure 5. Connection and signal conditioning for the coextruded filament.

as the polymer electrodes show significant electrical resistance. This resistance, connected in series between the voltage source (which is the piezoactive dielectric) and the amplifier, imposes an upper cut-off frequency f_{uc} of

$$f_{uc} = \frac{1}{2\pi R_s C_s} \quad (5)$$

where R_s is the electrode resistance and C_s is the sensor's intrinsic capacitance. It can thus be observed that the sensor's electrode resistance and intrinsic capacitance play a role in the output signal just for higher frequencies.

The amplifier gain at frequencies between the lower and upper cut-off frequency is determined by the feedback capacitance value, being inversely proportional to its value:

$$G = \frac{1}{C_f} \quad (6)$$

where

G = charge amplifier gain (V/C).

Equation (7) expresses the relation between electrical charge, capacity, and voltage in a capacitor

$$V = \frac{Q}{C} \quad (7)$$

with

V = voltage (V)

Q = electrical charge (C)

C = capacity (F).

The voltage at the amplifier's output is the voltage at the feedback capacitor, which is produced by the electrical charge moved by the sensor into the capacitor on mechanical excitation.

The output of the charge amplifier is finally connected to a National Instruments NI-6259 data acquisition board and custom-developed software based on Labview was used for signal acquisition, display and storage. The amplifier is supplied directly by the 5 V single supply of the data acquisition board and is provided with a 2.5 V offset to allow symmetrical signals to vary around the offset.

After proper grounding and shielding, the sensors produced a low-noise signal, which was improved by implementing in the software a 10th-order bandstop filter with a stopband between 45 and 55 Hz to reduce 50-Hz noise. With this setup the measurement system could represent even the smallest signals, in the order of a few mV, very accurately.

Measurement of Electrode Resistance. Although optimizing and characterizing in detail the conductivity of the polymer electrodes in the filament sensor is out of the scope of this work, some measurements were performed to assure that the conductivity provided by the electrode layers would not have an adverse effect on the signals produced by the sensor.

As discussed before, the electrode resistance influences the upper cut-off frequency of the sensor/amplifier response. The upper cut-off frequency depends both on the sensor's capacitance as well as on the electrode resistance [eq. (5)]. Sensors based on multiple filaments have been shown capacitances in the order of nanofarad and below.[30,31] In this work, just a single filament is used, which is shorter and thicker, thus possessing less electrode area and larger distance between electrodes. Consequently, less capacitance is obtained. Nevertheless, considering a parasitic capacitance of 1 nF, to achieve measurements up to 1 kHz, the maximum total resistance of the electrode layers of a sensor can be calculated as:

$$1\text{KHz} \leq \frac{1}{2\pi R_s \times 1\text{nF}} \quad (8)$$

$$R_s \leq 159\,\text{k}\Omega \quad (9)$$

As can be seen, and further considering that actual capacitance values are lower than 1 nF, the requirement for electrical conductivity is not very high from the signal conditioning point of view.

In the poling process, currents are very small. Electrode resistance should still be low enough to allow a sufficient electrical field to the whole PVDF layer for adequate poling. Ideally, the whole surface should be equipotential. Although this aspect has not been studied in detail in this phase of the research, the electrical resistance of the electrode layers has been characterized. Filaments were prepared in 20-cm segments, painted with conductive ink and contacted with crocodile clips for resistance measurement with a USAG 075 C multimeter. The distance between two ink settings was 10 cm, five samples were analyzed, and both the internal and the external conductive layers were measured.

Sensor Test Setup. The filaments were subjected to tensile stress to test its functionality as a mechanical sensor. For deformations along the filaments, these were placed between the grips (distance between grips: 30 mm) in a Shimadzu AG-IS 500 N universal tensile testing machine (Figure 6), using a load cell of 1 kN. A pretension was applied with the objective of keeping the filament permanently under tension during the test. From the mechanical characterization performed, it was decided to apply 5 N of pretension, a value sufficient for the purpose and lying well in the linear region of the strain–stress curve. The tester was set to pull the filaments with a displacement of 0.3 mm, corresponding to 1% of extension. The pulling speed was set to 100 mm min^{-1} and 20 cycles were performed.

Figure 6, right, shows the detail of connection. A fine clamp is used to connect the inner electrode. The outer electrode is contacted with the shield of the cable, which in turn is connected to ground, by means of a crocodile clip. The crocodile itself is not connected to anything; it just presses the cable shield against the outer layer of the filament.

RESULTS AND DISCUSSION

Extrusion

Figure 7 shows cross-section images of two samples of Type 1 and Type 2 filaments each. To obtain the images, the filaments were placed into resin, a cross-sectional cut was done and the resin was polished. The pictures were then taken with a Leica

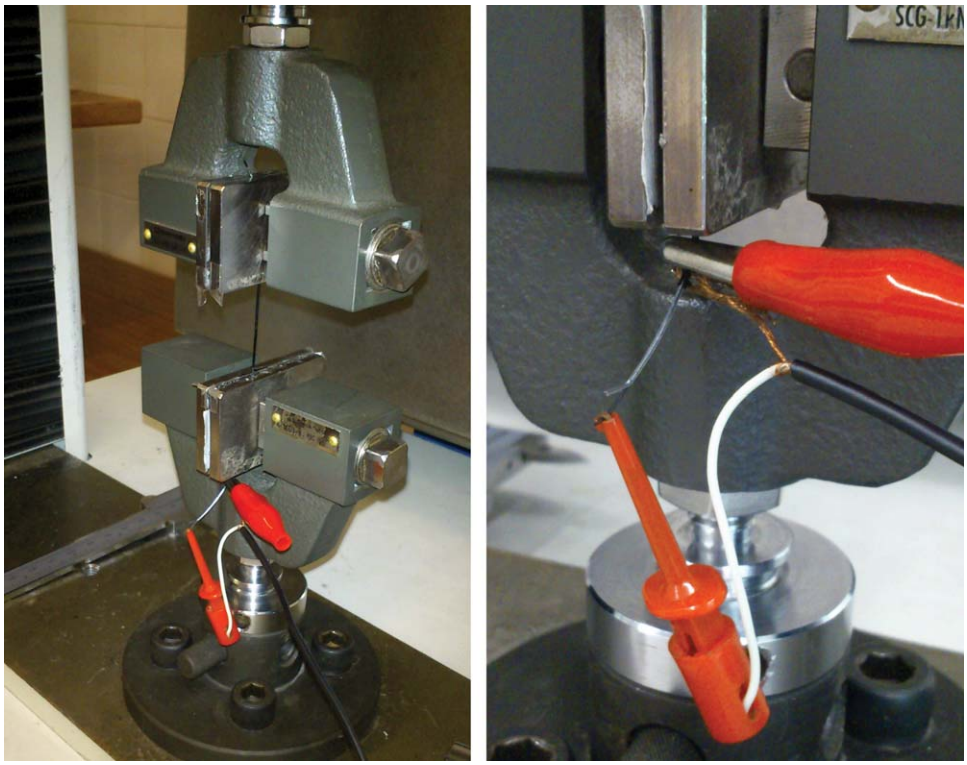

Figure 6. Test setup for drawing action (left), electrical connection detail (right). [Color figure can be viewed in the online issue, which is available at wileyonlinelibrary.com.]

DFC 280 digital camera connected to an Olympus BH2 reflection microscope.

Five cross sections of each type of filaments were analyzed. Filament and layer thickness were observed to be stable within about 10% of the average values, for the cross-sections analyzed and for the processing conditions defined. As for the geometry, the examples given are representative of the obtained variability. As can be observed, the shape of the layers is not fully axisymmetric, with Type 2 filaments exhibiting a more even geometry than Type 1 filaments. A slight variation in shape is also accompanied by varying adhesion between the layers. A larger trend for layer delamination is observed for Type 1 filaments.

Although the modular design of the dye appeared as an interesting advantage of the extrusion die, fine interplay between the different modules is required, which revealed itself as a source of imprecision. The inexistence of a tuning mechanism and the complex rheological behavior of the materials used, render process control very difficult to achieve, resulting in the obtained asymmetric layer distribution and slight variations. Still, it was possible to obtain continuous layers of the different materials that comprise the filament, which assures electrical conductivity in the inner and outer layers, making it possible to pick-up the electric signals generated in the piezoelectric layer. It was not possible to produce thinner filaments under stable conditions.

A more even geometry of the filament would allow improvement in several aspects, among them the optimization of the poling procedure as, for example, the maximum electric field that can be applied, which is currently imposed by localized defects of the PVDF layer. However, an on-line tunable tool, required to handle different materials, layer thickness distribution, and processing conditions, would have a prohibitive cost, not adequate for this phase of the investigation (proof of concept).

Another problem to be tackled is the lack of adhesion between the conductive and the electroactive areas, which can reduce the signal pick-up of the sensor and thus decrease its sensitivity and affect the homogeneity of behavior along the filament length. Although the void spaces visible in the microscopic images are most probably caused by the cutting and polishing actions used in sample preparation, they reveal a potential for layer delamination.

Poling Fields

Table II summarizes the approximate PVDF layer thickness measured from the two samples presented in Figure 7, and under a voltage of 9 kV, the resulting poling field for the thickest and thinnest points of the PVDF layer.

As can be seen, these are in the order of poling fields used in another work for PVDF filament poling, but still below optimal values as reported elsewhere, allowing still an optimization of the output signal.[1,11,30]

Currents measured during the poling process are in the order of tens of milliamperes. As will be presented later in this section, the electrode layer resistance is in the order of tens of kiloohm at most. This means that a voltage drop of a few hundred volts can be expected at most between the connection of the voltage

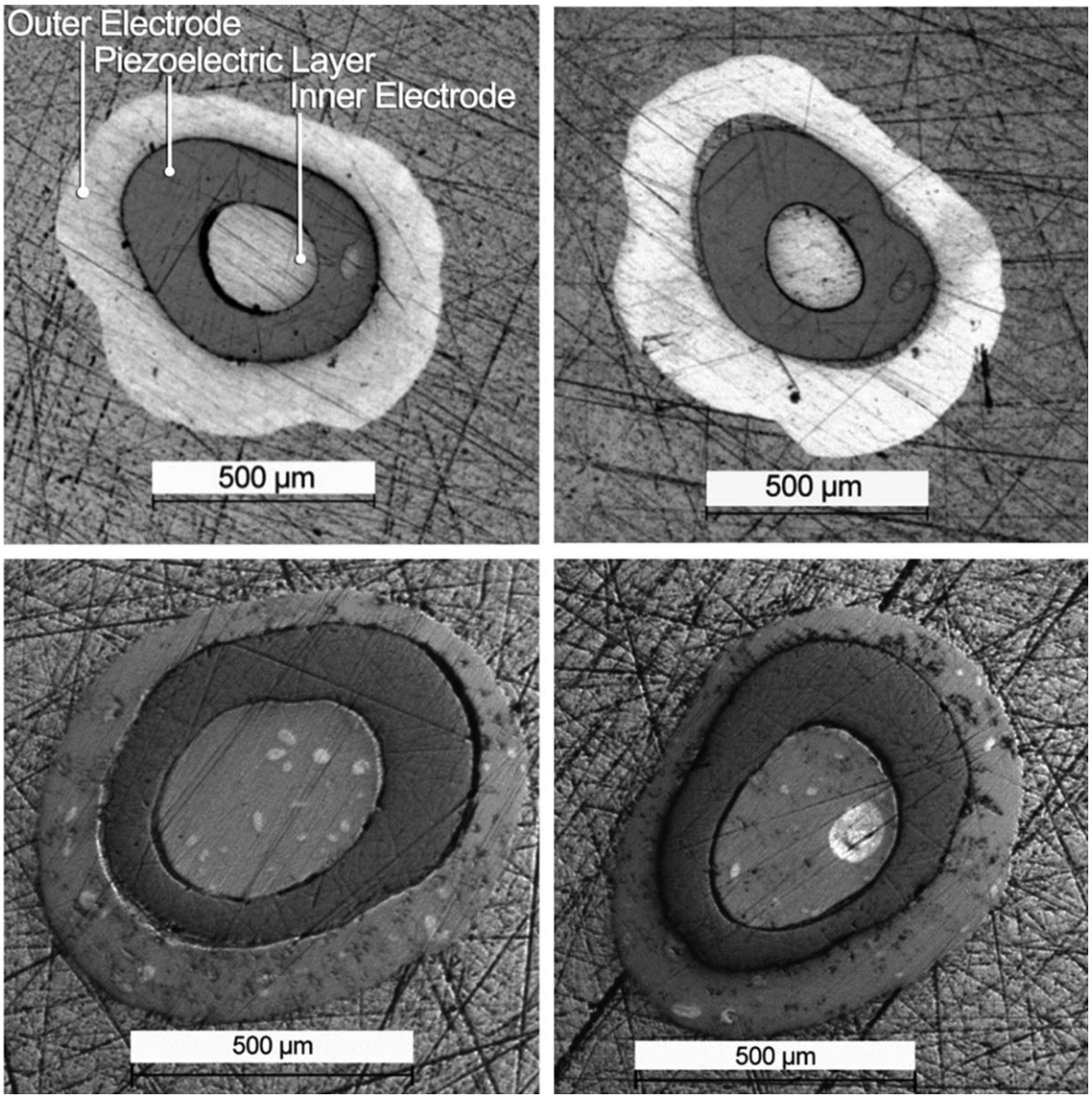

Figure 7. Microphotographs of the three-layer filament cross section in two samples of filament Type 1 (upper row) and two samples of filament Type 2 (lower row).

source and the farthest point of the filament. Although not very significant for the poling of the 10-cm long filaments used, this voltage drop may be important when poling longer filaments through contact poling. In fact, this is very important for industrial production, where it is desirable that a large amount of filament can be poled in one step. This subject has to be analyzed with more detail, because there is the possibility that the measured currents are surface currents not affecting the electrical potential present at the bulk of the electrode volume. If the production of an equal potential along the whole electrode turns out problematic, other poling methods, such as Corona poling and application of an electric field during the drawing step can be explored. However, the application of these methods to three-layered filaments, in which the outer electrode covers the PVDF layer that is to be poled, presents new challenges when compared to poling simple PVDF monofilament or two-layered structures.[27,28,31]

β-Phase Content

Figure 8 shows the FTIR spectrum obtained for the different filaments.

The calculation of β-phase content according to eq. (2) yields the result presented in Table III.

The value found for the Type 1 filament is relatively low, considering that in previous experiments with PVDF extruded filament, piezoelectric phase contents of 70–80% had been achieved.[20] Still, this percentage of β-phase material is sufficient to obtain electroactive filaments, as will be presented in Section Electrical Tests.

Conversely, the value of approximately 68% found for the Type 2 filament confirms that, under the current dynamic processing conditions, the high heater temperature is not inhibiting the achievement of electroactive phase material.

Table II. PVDF Layer Thickness and Poling Fields

Filament	Minimum thickness (μm)	Maximum thickness (μm)	Minimum field (MV m^{-1})	Maximum field (MV m^{-1})
Type 1	91	200	47	86
Type 2	47	160	56	190

The higher values of β-phase content obtained for the Type 2 filaments are also related to the higher draw ratio, which was 5, whereas the one achieved for the Type 1 filaments was 4.

Mechanical Test

Figure 9 shows the results of the tensile test.

The graph shows that Type 2 filaments exhibit almost double the breaking strength of Type 1 filaments. In both cases, rupture occurs at values that are much higher than the force ranges in which the filament sensor is expected to be used (lower than 20 N). Moreover, the filaments exhibit linear stress–strain behavior in this range.

It can also be observed that the tensile modulus is higher for the filament Type 2. The difference in mechanical behavior results mainly from the higher draw ratio used in filament Type 2, as the cross-section area of both filaments is very similar.

Regarding Type 1 filaments, layers break at different times. The outer layer is the first to break, followed by the PVDF intermediate layer, which then causes sample fracture.

For Type 2 filaments a different behavior is observed. These samples fully fracture almost immediately after the failure of the first layer, which is also the outer conductive layer. The mechanical properties of the layers seem in this case to be more balanced in terms of mechanical resistance.

Rupture of the innermost layer cannot be observed on the graph. This layer seems to be already broken when the PVDF layer breaks.

Electrical Tests

Measurement of Electrical Conductivity. As stated previously, the optimization and detailed study of the conductive layers is out of the scope of this work. Nonetheless, some results are presented, as they are relevant for evaluation of the sensors performance.

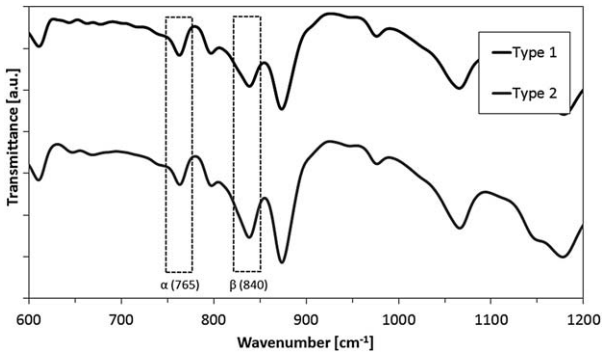

Figure 8. FTIR spectrum of the extruded samples.

Table III. β-Phase Content of the Samples

Filament	% β-phase content	Standard deviation (%)
Type 1	59	3.6
Type 2	68	6.5

Figure 10 shows the conductance measured for the external electrode layer in 10-cm long segments of Type 1 filaments, as a function of drawing temperature and ratio. For easier graphical representation, conductance values instead of resistance are displayed. Points with zero conductance represent samples for which the resistance value was out of the range of the used multimeter (>20 MΩ).

It is interesting to note the increase of conductance with drawing temperature and the expected decrease with draw ratio. For the selected process parameters of drawing at 210°C and draw ratio of $R = 4$, the resistance of the 10-cm long external layer is about $R = 1/80\ \mu S = 12.5\ k\Omega$. Values for the internal layer follow the same trends and are in the same order of magnitude, although about two times higher for the produced geometry.

The production of filaments using the Nanocyl compound required the decision on the percentage of conductive filler to be used. Preliminary experiments showed that only using a minimum of 5 wt % filler content could assure conductivity in the order of magnitude of the ones presented for Type 1 filaments. The compound was then prepared with 7 wt % of filler. Figure 11 shows the results of the conductance for these types of filaments.

The same observations regarding influence of drawing ratio and temperature apply here, but in this case, it has been possible to achieve higher draw ratios.

For the selected process parameters of drawing at 210°C at a draw ratio of $R = 5$, the resistance of the 10-cm long external layer is about 40 kΩ. Values for the internal layer follow the same trends and are in this case very similar to the ones measured for the outer layer, which results from a better balance between the inner and outer layer's dimensions in this case. The requirement for maximum resistance defined is also fulfilled in this filament type.

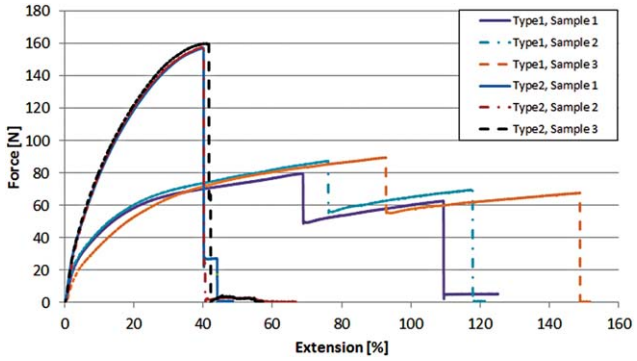

Figure 9. Tensile test on samples of the filaments. [Color figure can be viewed in the online issue, which is available at wileyonlinelibrary.com.]

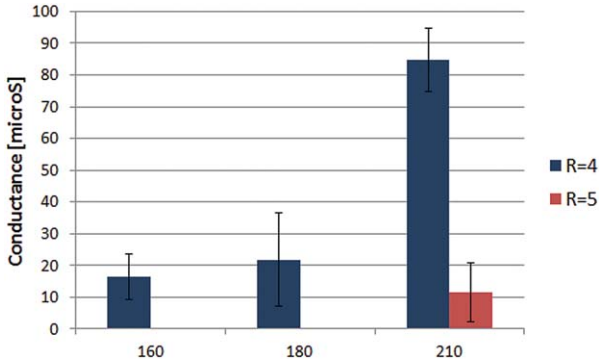

Figure 10. Conductance of 10-cm long external electrode layer samples in filament Type 1, as a function of drawing ratio and temperature. [Color figure can be viewed in the online issue, which is available at wileyonlinelibrary.com.]

Electromechanical Response. Figure 12 shows the force/displacement values measured by the universal tester and the electrical signals resulting from this excitation, for a sample of filament Type 1.

The same is shown in Figure 13 for a sample of filament Type 2.

As can be observed in Figures 12 and 13, the electrical response depicts the force variations very accurately, with the typical effects present on a piezoelectric sensor coupled to a charge amplifier, as explained in Section Measurement of Electrical Conductivity. The signal suffers a decay of average value caused by the high-pass response of the charge amplifier, which eliminates the average values over time (the signal tends to the electrically produced 2.5 V offset). After the last cycle, the signal again converges to the 2.5 V offset. These two decays occur with a time constant that, in the current case and considering the values of $C_f = 10$ nF and $R_f = 100$ MΩ, is $T = 1$ s, which is in accordance with the observed signals. From these values, the lower cut-off frequency f_{lc} of the charge amplifier can be calculated, according to eq. (4), as being 0.16 Hz.

The peak-to-peak value of the electrical signal at Cycle 11 for filament Type 1 is 0.97 V, corresponding to a force variation of

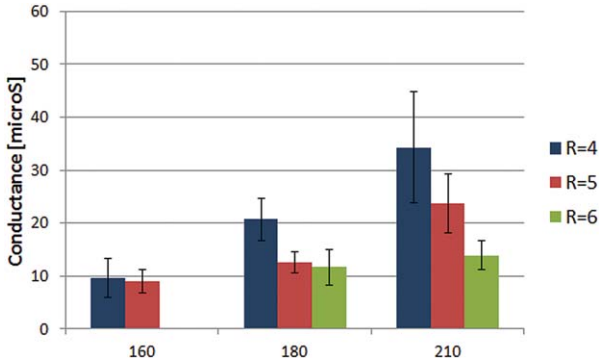

Figure 11. Conductance of 10-cm long external electrode layer samples in filament Type 2 filled with 7 wt % of CNT, as a function of drawing ratio and temperature. [Color figure can be viewed in the online issue, which is available at wileyonlinelibrary.com.]

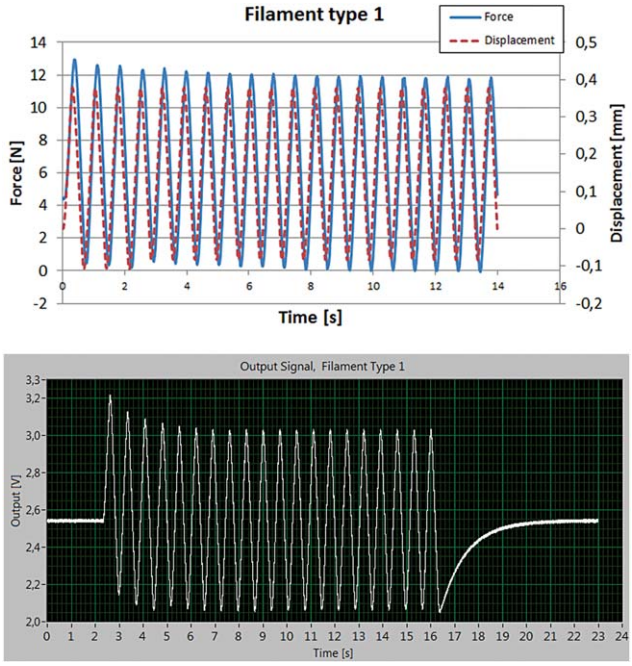

Figure 12. Force and displacement (upper graph) and electrical signal (lower graph) picked up by the measurement system during the cyclic test on one sample of filament Type 1. [Color figure can be viewed in the online issue, which is available at wileyonlinelibrary.com.]

11.78 N. Filament Type 2 presents 1.44 V for 19.41 N. For these values, the sensitivities of the sensors are computed as follows:

The charge injected into the capacitor for a force range of 11.78 N in filament Type 1 is

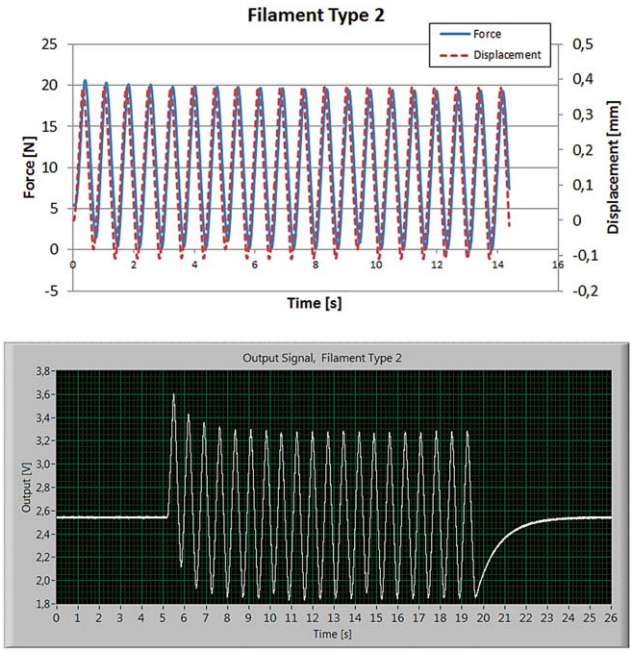

Figure 13. Force and displacement (upper graph) and electrical signal (lower graph) picked up by the measurement system during the cyclic test on one sample of filament Type 2. [Color figure can be viewed in the online issue, which is available at wileyonlinelibrary.com.]

$$Q = V \times C = 0.97 \times 10 \times 10^{-9} = 9.7\ \text{nC} \quad (10)$$

For filament Type 2, a value of 14.4 nC is obtained.

Thus, the sensitivity of the filament sensor Type 1 can be calculated as:

$$S = \frac{Q}{F} = \frac{9.7 \times 10^{-9} C}{11.78} = 0.82 \frac{\text{nC}}{\text{N}} \quad (11)$$

The same calculation results in 0.75 nC N^{-1} for filament Type 2.

For comparison, a sensor based on commercial PVDF film (metallized film sheet from Measurement Specialties, 28-μm thickness), with similar volume of PVDF, was prepared. A strip of the PVDF film with dimensions 30 × 7 mm^2 was cut. The tensile testing machine was set to produce the same cyclic extension of 1% in the longer direction of the strip and the electrical output of this sensor was measured using the same charge amplifier. The signal produced by this sensor was much higher and a feedback capacitor of 104 nF had to be used to lower the amplifier gain and avoid saturation. In this configuration, the measurement system produced 1.95 V for a force variation of 6.1 N. Repeating the calculation of eqs. (10) and (11), the output of the film-based sensor results as 33.2 nC N^{-1}, which is an order of magnitude higher than that produced by the filaments.

To obtain an estimation of the piezoactive material's piezoelectric coefficient, the d_{1r} coefficient is calculated as follows:

$$d1r = \frac{Q_r / A_{el}}{F_3 / A_{cr}} \quad (12)$$

with

Q_r = charge displaced in direction r (C)

A_{el} = electrode area (m^2)

F_3 = force applied in direction of axis 1 (N)

A_{cr} = cross-sectional area of the filament (m^2).

For the parallel configuration found in film sensors, the calculation is straightforward, but for the filament sensor the inner and outer electrode areas are different. The exact implications of this fact would have to be studied in more detail. For the purpose of this study, the average between inner and outer electrode areas is considered. Based on the cross sections displayed in Figure 7, typical electrode and cross-sectional areas were calculated. Using these values and the electrical response values previously presented, d_{1r} coefficients of 3.59 and 2.78 pC N^{-1} are obtained. The same calculation yields d_{31} = 31.03 pC N^{-1} for the piezoelectric film.

Several factors should be taken into account to explain the difference in sensitivity of the filament sensors when compared to the film. In the first place, the β-phase contents of 59 and 68% found in the filaments are lower. β-phase content of 95% has been determined in poled piezoelectric film from the same manufacturer.[37] Second, poling fields achieved in this experiment are also low. Although they exceed the coercive field for optimal results a larger poling field is required.[1,11] To increase the poling field, a more even geometry of the filament has to be achieved. This would allow increasing the poling voltage. In combination with this, better results may be achieved by reducing the PVDF layer thickness.

A third issue that may affect the results obtained is the adhesion between the electrical conductive layers and the PVDF layer. As can be observed in Figure 7, there is a potential for layer delamination and the occurrence of voids between conductive layers and the electroactive layer. This affects the collection of the electrical charge moved to/from the surface of the PVDF by the piezoelectric effect, reducing the signal produced in the charge amplifier and thus decreasing sensitivity.

Considering the higher β-phase content, poling field, and slightly larger volume of electroactive material present in filament sensor Type 2, a higher sensitivity from this sensor would be expected, which did not occur. Considering all the plausible factors for this fact, lack of layer adhesion is seen as a probable cause for sensitivity loss and should be improved in subsequent studies.

CONCLUSIONS

In this work, a proof-of-concept for a three-layered coextruded filament sensor, produced in a continuous manner, has been given. The experimental characterization performed showed that the sensor produces an electric signal proportional to the tensile force applied.

Conditions have been set for extrusion and drawing of the filaments to provide the electroactive layer with its piezoelectric properties. Two different types of materials for the conductive layers of the filaments have been tested. The electroactive phase (β-phase) content of the filaments has been measured using FTIR and found to be of 59 and 68% for Type 1 and Type 2 filaments, respectively.

The filament has been tested under tensile stress and its functionality as a sensor has been demonstrated. Three centimeter long sections of the filaments exhibited a sensitivity of 0.82 and 0.75 nC N^{-1}. A sensor of approximately equal volume of PVDF based on a commercial PVDF film provided 33.2 nC N^{-1}. Albeit this difference, the filament sensor provides enough sensitivity to generate high quality signals suitable for the development applications.

Further work on optimization of the extrusion process can improve the sensitivity and geometry of the sensor. The reduction of the filament's cross-sectional dimensions can then lead to the mass production of low-cost electroactive materials with possibility of full textile integration and interesting sensing capabilities and applications.

The production of three-layered filaments provides fully functional filamentary sensors that can be integrated into a wider sensing structure or used by themselves. In other works, one or both electrodes have to be provided through further preparation.[27–31]

The possibility of poling the filaments inline would be also an important advantage that should be considered in future work.[27,28,31] Although in this study only short filament segments have been tested, the final goal is the production of functional

filament sensors in large amounts, either already poled during the production process, or poled in batches of sufficient size to allow keeping costs low.

ACKNOWLEDGMENTS

This work was supported by FEDER through the COMPETE Program and by the Portuguese Foundation for Science and Technology (FCT) by project PTDC/CTM/108801/2008 | FCOMP-01-0124-FEDER-009480 and in the framework of the Strategic Project PEst-C/FIS/UI607/20112011, PEst-C/CTM/LA0025/2013 (Strategic Project-LA 25-2013-2014), and PEst-C/CTM/UI0264/2011. Authors also thank the project Matepro–Optimizing Materials and Processes," ref. NORTE-07-0124-FEDER-000037," cofunded by the "Programa Operacional Regional do Norte" (ON.2–O Novo Norte), under the "Quadro de Referência Estratégico Nacional" (QREN), through the "Fundo Europeu de Desenvolvimento Regional" (FEDER).

REFERENCES

1. Martins, P.; Lopes, A. C.; Lanceros-Mendez, S. *Prog. Polym. Sci.* **2014**, *39*, 683.
2. Bauer, S. *J. Appl. Phys.* **1996**, *80*, 5531.
3. Nalwa, H. S. In Ferroelectric Polymers: Chemistry, Physics and Applications; Marcel Dekker: New York, **1995**.
4. Salimi, A.; Yousefi, A. A. *Polym. Test.* **2003**, *22*, 699.
5. Lanceros-Mendez, S.; Mano, J. F.; Costa, A. M.; Schmidt, V. H. *J. Macromol. Sci. Part B: Phys.* **2001**, *40*, 517.
6. Nakamura, K.; Sawai, D.; Watanabe, Y.; Taguchi, D.; Takahashi, Y.; Furukawa, T.; Kanamoto, T. *J. Polym. Sci. Part B: Polym. Phys.* **2003**, *41*, 1701.
7. Lanceros-Mendez, S.; Moreira, M. V.; Mano, J. F.; Schmidt, V. H.; Bohannan, G. *Ferroelectrics* **2002**, *273*, 15.
8. Matsushige, K.; Nagata, K.; Imada, S.; Takemura, T. *Polymer* **1980**, *21*, 1391.
9. Gregorio, R., Jr.; Ueno, E. M. *J. Mater. Sci.* **1999**, *34*, 4489.
10. Gregorio, R., Jr.; Cestari, M. *J. Polym. Sci. Part B: Polym. Phys.* **1994**, *32*, 859.
11. Gomes, J.; Nunes, J. S.; Sencadas, V.; Lanceros-Mendez, S. *Smart. Mater. Struct.* **2010**, *19*, 065010.
12. Sencadas, V.; Gregorio, R., Jr.; Lanceros-Mendez, S. *J. Macromol. Sci. Part B: Phys.* **2009**, *48*, 514.
13. Dickens, B.; Balizer, E.; DeReggi, A. S.; Roth, S. C. *J. Appl. Phys.* **1992**, *72*, 4258.
14. Dargaville, T.; Celina, M.; Elliott, J.; Chaplya, P.; Jones, G.; Mowery, D.; Assink, R.; Clough, R.; Martin, J. Characterization, performance and optimization of PVDF as a piezoelectric film for advanced space mirror concepts, SANDIA REPORT SAND2005–6846; Sandia National Laboratories: CA, **2005**.
15. Measurement Specialties. Piezo Film Sensors Technical Manual, Application Note; Measurement Specialties, **2008**, p 43. Available at: http://www.meas-spec.com/downloads/Piezo_Technical_Manual.pdf, accessed on March 26, 2014.
16. Moore, E. P., Jr. In Polypropylene Handbook, 1st ed.; Hanser: New York, **1996**.
17. Naficy, S.; Garmabi, H. *Compos. Sci. Technol.* **2007**, *67*, 3233.
18. Hua, Z.; Ping, R.; Guifang, Z.; Changfa, X. *J. Wuhan Univ. Technol. Mater. Sci. Ed.* **2006**, *21*, 53.
19. Steinmann, W.; Walter, S.; Seide, G.; Gries, T.; Roth, G.; Schubnell, M. *J. Appl. Polym. Sci.* **2011**, *120*, 21.
20. Lund, A.; Hagström, B. *J. Appl. Polym. Sci.* **2010**, *116*, 2685.
21. Ferreira, A.; Costa, P.; Carvalho, H.; Nóbrega, J. M.; Sencadas, V.; Lanceros-Mendez, S. *J. Polym. Res.* **2011**, *18*, 1653.
22. Lund, A.; Hagström, B. *J. Appl. Polym. Sci.* **2011**, *120*, 1080.
23. Glauss, B.; Steinmann, W.; Walter, S.; Beckers, M.; Seide, G.; Gries, T.; Roth, G. *Materials* **2013**, *6*, 2642.
24. Janiczek, T. *J. Electrostat.* **2001**, 51–52, 167.
25. Mazurek, B.; Różecki, S.; Kowalzcyk, D. In Proceedings of the 6th International Conference on Properlies and Applications of Dielelectric Materials; Xi'an Jiaotong University: China, **2000**; p 1041.
26. Mazurek, B.; Różecki, S.; Kowalczyk, D.; Janiczek, T. *J. Electrostat.* **2001**, 51–52, 180.
27. Vatansever, D.; Hadimani, R. L.; Shah, T.; Siores, E. In Proceedings of the International Congress of Innovative Textiles, ICONTEX 2011, Istanbul, **2011**.
28. Hadimani, R. L.; Vatansever, D.; Sion, N.; Shah, T.; Qian, L.; Shi, S.; Siores, E. *Smart. Mater. Struct.* **2013**, *22*, 075017.
29. Walter, S.; Steinmann, W.; Schütte, J.; Seide, G.; Gries, T.; Roth, G.; Wierach, P.; Sinapius, M. *Mater. Technol. Adv. Perform. Mater.* **2011**, *26*, 140.
30. Lund, A.; Jonasson, C.; Johansson, C.; Haagensen, D.; Hagström, B. *J. Appl. Polym. Sci.* **2012**, *126*, 490.
31. Nilsson, E.; Lund, A.; Jonasson, C.; Johansson, C.; Hagström, B. *Sens. Actuators A Phys.* **2013**, *201*, 477.
32. Egusa, S.; Wang, Z.; Chocat, N.; Ruff, Z. M.; Stolyarov, A. M.; Shemuly, D.; Sorin, F.; Rakich, T.; Joannopoulos, J. D.; Fink, Y. *Nat. Mater.* **2010**, *9*, 643.
33. Abouraddy, A. F.; Bayindir, M.; Benoit, G.; Hart, S. D.; Kuriki, K.; Orf, N.; Shapira, O.; Sorin, F.; Temelkuran, B.; Fink, Y. *Nat. Mater.* **2007**, *6*, 336.
34. Lanceros-Mendez, S.; Mano, J. F.; Costa, A. M.; Schmidt, V. H. *J. Macromol. Sci. Phys.* **2001**, *40*, 517.
35. Gautschi, G. In Piezoelectric Sensorics: Force, Strain, Pressure, Acceleration and Acoustic Emission Sensors, Materials and Amplifiers; Springer-Verlag: Berlin, **2002**.
36. Karki, J. Signal conditioning piezoelectric sensors, Application Report SL0A033A; Texas Instruments, September, 2000. Available at: http://www.ti.com.cn/cn/lit/an/sloa033a/sloa033a.pdf, accessed on March 26, 2014.
37. Sencadas, V.; Costa, C. M.; Moreira, V.; Monteiro, J.; Mendiratta, S. K.; Mano, J. F.; Lanceros-Méndez, S. *e-Polymers* **2005**, *2*, 1.